Preprint Title Effect of Power Law-Index for Accurate Natural Frequencies of Rotating Isotropic SWCNTs with Ring Supports

Authors Muzamal Hussain and Muhammad Nawaz Naeem

Article Type Full Research Paper

ORCID® iDs Muzamal Hussain - https://orcid.org/0000-0002-6226-359X

Effect of Power Law-Index for Accurate Natural Frequencies of Rotating Isotropic SWCNTs with Ring Supports

Muzamal Hussain[1] and Muhammad Nawaz Naeem[2]*

[1]Research scholar, Department of Mathematics, Govt. College University Faisalabad, 38000, Faisalabad, Pakistan

[2]Professor, Department of Mathematics, Govt. College University Faisalabad, 38000, Faisalabad, Pakistan

To whom correspondence and proof should be sent: Dr. Muzamal Hussain, Department of Mathematics, Government College University Faisalabad (GCUF), Allama Iqbal Road, Faisalabad 38040, Pakistan, Tel: +92-41-9330005; Fax: +92-41-9201419

[*]E-mail: muzamal45@gmail.com; muzamalhussain@gcuf.edu.pk

Abstract

Vibration analysis of carbon nanotubes (CNTs) is very essential field owing to their many promising applications in tiny instruments. The unique and interesting properties of CNTs, particularly their mechanical and electrical features, have fascinated industries and researchers to implement CNTs for production of different electromechanical devices. Research on vibration behavior of CNTs was done for a few decades ago. Vibrations of isotropic rotating zigzag and chiral single-walled carbon nanotube (SWCNTs) with ring supports are established using the Love's shell theory. To discretize the governing equations of current model, Galerkin's method is utilized for frequency equations of single-walled carbon nanotubes (SWCNTs). The unknown axial functions have assumed by characteristic beam functions which fulfill boundary conditions applied at the tube ends. Effects of different parameters with ring supports on the fundamental natural frequencies versus ratio of length-to-radius, angular speed and height-to-radius ratio have been investigated. The frequencies curves decrease as the length-to-diameter ratio increases. With the increase of angular speed the frequency curve of backward waves increases and forward wave decreases for rotating zigzag and chiral tubes. On the other hand, the phenomena of frequency versus height-to-radius ratio are counterpart of length-to-radius ratio for rotating boundary conditions. The frequency phenomena have been observed very pronounced with ring

support. Frequency value of C-C end condition is higher than those of C-F computations. The results of single-walled carbon nanotube are computed by using MATLAB software. To validate the accuracy of present model, the results have been compared with earlier modeling/simulations.

Keywords

Rotating, carbon nanotube, FGM, vibration, energy variational procedure.

1. Introduction

Carbon is one of the most versatile elements that is found in nature, owing to exceptional characteristics, potential applications and substantial impressions on the industry. Carbon is found in its miscellaneous forms of diamond, graphite and polymers, which are very important for our lives. Since the discovery of CNTs, has become very important and interest of research due to considerable observation and research publications every year. CNTs have a variety of uses and applications in potential looking fields, some of which are charge detectors, electronics, communication, composite materials, biotechnology, environment, energy storage, chemical, and optical [1]. Therefore, in order to effectively use of CNTs in each of these fields, it is important that their vibration characteristics are examined. Owing to the small sizes of the micro beams, they are very appropriate for designing small instruments like sensors and actuators [2, 3]. There is considerable use of rotating tubes in different areas such as high power engine, magnetic shields, civil, mechanical and aerospace engineering [4-11]. The important application of the current investigation of rotating FG-CNT is in nano-engineering structure like a sensors and actuators.

In last fifty years, many theories have been presented for vibration of rotating and non-rotating shells[1,2,5,9,12] and shells with ring support [13,14–21]. Reddy and co-authors investigated the bending, longitudinal, nonlinear, free and shear flexible vibration of FG porous microplates, nanobeams and carbon nanotubes within elastic medium using modified coupled theory, differential quadrature (DQM) and finite element method (FEM) [22,23,24,25]. Moreover, these authors modified the plate theories in a very clear manner that is based on diverse nonlocal theory of elasticity. Many investigators studied the buckling and post buckling

of nano structure as nano-plates and –beams [26–33]. On the other side, due to the practical importance of vibration of rotating CNTs is very sparse.

Mouffoki et al. [34] studied the vibration of nanobeam using novel deformation theory resting on the elastic foundation. The influence of deformation theory is observed with displacement field and concluded that classical theory is less than beam theory. Wuite and Adali [35] studied the behavior of one dimensional CNT using multi-scale analysis. Effect of different parameters and volume fraction of CNT with diameter was examined. Bouafia et al. [36] and Bounouara et al. [37] used 3D-nonlocal theory to calculate the frequency characteristics of nano-beams and -plates. The effects of strain and shear factor across the thickness was considered. These studies have an effective analysis and design of nano-structures. Ebrahimi et al. [38] used porous electro-elastic properties to calculate the vibration using deformation plate theory. These properties vary in the direction of thickness. Hamilton's principle was used to derive the governing equation for FG plates. Zemri et al. [39] and Ahouel et al. [40] presented buckling, bending and vibration of nano-beams with different nonlocal Eringens relation. These models capturing the matrial parmeters with varying the thickness. Gao et al. [41] investigated the free vibration of porous material with little amount of graphene platelets using different boundary conditions. The parent metal was reinforced by four different distributions with Young's modulus and shear modulus. Hussain et al. [42] assessed the fundamental natural frequencies frequencies (FNF) of SWCNTs using wave propagation approach based on Donnell shell theory. The effect of in-plane rigidity and mass density per unit lateral area with different indices of armchair and zigzag was considered.

Zhou et al. [43] developed flutter characteristic of plates using classical boundary conditions. According to shear deformation theory, with the conjunction of heat conduction was used to calculate the distribution of temperature in thickness direction. Hussain and Naeem [44,45] used different theories to examine the vibration of SWCNTs with wave propagation approach. The effect of length and thickness was observed against frequency. Also the influence of dimensionless frequency was investigated with armchair and zigzag indices for in-plane rigidity and mass density lateral area. Żur [46] presented the classical plate theory to investigate the numerical results of free- and non-axisymmetric results of annular plates. The governing equation of plates was utilized with the help of quasi-Green's function. The vibration of these plates has been calculated with clamped-clamped and simply supported boundary conditions.

The vibration of sandwich nanoplates was observed to investigate the buckling, bending, and stability analysis in detail using deformation, trigonometric and hyperbolic and nonlocal theories [41,47,48,49,50,51,52,53,54].

Shen [55] presented nonlinear bending behavior of single-walled carbon nanotubes with simply supported edge condition. The molecular dynamic simulation was used to obtain the material properties of single-walled carbon nanotubes using perturbation technique. Ke et al. [56] incorporated the free vibration of SWCNT using Timoshenko beam theory and controlling equation of motion was derived using the Ritz-method. The thickness of SWCNT was governed by the rule of mixture with different support conditions. Some material researchers [57,58,59] assumed the straight and aligned SWCNT resting on elastic foundation with thermal environment. The effects of in-plane rigidity, temperature and volume fraction was calculated with sheets. Aragh et al. [60] investigated the vibration of CNT based on cylindrical shell panel using Eshelby-Mori-Tanaka approach. The volume fraction was considered in the direction of thickness and constitutive law was used to examine the vibration frequencies of SWCNTs. Żur [61] studied the abstract analysis of plates for free and non- axisymmetric vibration with ring supports using classical theory. The quasi- Green function was used for the solution of boundary value problem using different boundary conditions. Rafiee et al. [62] applied the Euler-Bernoulli beam theory with the conjunction of Kármán geometric theory. Wattanasakulpong and Ungbhakorn [63] employed shear deformation to calculate bending and vibration characteristics of CNT resting on Pasternak foundation. With the help of mixture rule, the SWCNTs are mixed with polymeric matrix. Shahsavari et al. [64] used Galerkin's method to calculate the free vibration of porous plates placed on elastic foundations. A novel hyperbolic theory of quasi-3D was used for the porosity distribution and patterns. Murmu and Adhikari [65] studied non-local effect of rotating structure for practical development using non-local Euler theory. For undergoing motion with the molecular hub, the carbon nanotube is assumed to be attached.

Vibration of rotating isotropic CNT is very rare. Some researchers used first time to investigate the rotating vibration of Shells [See Refs.66,67,68,69,70]. Moreover, the behavior of vibrating isotropic CNT has been studied in recent years [71,72,73]. As far as the author's knowledge goes, vibrational behavior of rotating isotropic CNT using Galerkin's method has not been investigated/assumed.

In addition, for the vibration of CNTs, many researchers have used different numerical techniques; for example modified coupled theory [22], 3D-nonlocal theory [36,37,64] differential quadrature method [23,41], wave propagation approach [42,44,45] finite element method [24] classical theory [34], deformation and shear deformation theory [38,43] ,nonlocal theory [39,40], quasi-Green's function [46,61] and other techniques [41,49,50,53,54]. For example, CNTs can be modeled as one dimensional Euler-Bernoulli beams [34,36,37]. More refined continuum mechanics solutions especially at high frequencies was obtained via Timoshenko beam model (TBM) and other theories [18,38,43,56], which includes shear and rotary inertia of the beam. It is necessary to employ TBM to capture the rotary inertia effects and shear deformation and provide accurate prediction for smaller length-to-diameter ratio of CNT, but have several computational problems are detected due to its conceptual simplicity. The TBM cannot capture the cross-sectional deformation of CNTs and, mathematically, TBM only provides a limit of large number of modes and frequency production.

The proposed method is a better and popular tool to investigate the overall vibration of SWCNTs. Vibration characteristics of single- and double-walled CNTs were conducted using flexible shell model [9,12,13,25,21]. Hussain et al. [42] and Hussain and Naeem [44,45] has used cylindrical shell model using wave propagation in SWCNTs to establish the new innovative techniques. Moreover, a new novel theoretical model gives innovative computational results for the vibration of CNTs, than earlier models [13,22,24,25,37,38,53,54,61,75-78]

In present work, we analyze the vibrations of isotropic rotating single-walled carbon nanotube (SWCNTs) with ring supports using Love shell theory based on Galerkin's method, which is our particular motivation. Since there is no evidence in the literature regarding present model where such problem have been studied. Two forms of SWCNTs, viz zigzag and chiral are considered for their vibration characteristics using with ring supports versus different parameters and boundary conditions. This is also our motivation for carrying out the present work.

The main objective of present work is used to investigate the fundamental frequency of rotating isotropic SWCNTs with ring supports under polynomial volume fraction law with clamped-clamped and clamped-free boundary conditions. In our case, the Galerkin's method is applied to solve the presented tube dynamics equations and we have formulated the tube frequency equation in the eigenvalue form. This proposed model are quite straight forward for the vibrational analysis of these structures of SWCNTs. Effects of different parameters on

fundamental natural frequencies versus ratios of length- and height-to-radius and angular speed are investigated. It is found that on increasing the ratio of length-to-radius, the resulting frequencies decreases and with the increase of height-to-radius ratio the frequencies increases. It has been shown that on enhancing angular speed, both backward and forward waves increases and decreases respectively. It is also found that on enhancing the position of ring supports, the frequency curves increase in the start and at the mid are higher and at the last the frequencies are same as the frequencies was observed in the start of attached ring supports. Frequency value of C-C end condition is higher than those of C-F computations. It is investigated that the frequencies of zigzag (5, 0) are lower than those of FNFs of (9, 0) and it is found that frequency outcomes of chiral (9, 5), are higher than those of (6, 4). Subsequently, the validation study has been performed through the available published literature. The results of single-walled carbon nanotube have been computed by using MATLAB software. To discretize the governing equations of present model into frequency equations of SWCNTs, Galerkin's method is used.

2. Polynomial volume fraction law

In carbon nanotubes (CNTs), the constitutes material for modeling can be done with various function of distribution, is termed as mixture rule. The mathematical modeling of CNTs, power law function of along thickness direction has been used and the various properties such as coefficient of thermal conductivity and expansion of the CNTs and ceramic material (AL203). The variation in temperature and properties has been gained using volume fraction and temperature. In accordance of power law in the thickness direction, the fraction volume changes as [24]. Upon evaluation of the total volume fraction of CNTs V_{tcnt} across the tube thickness, it is revealed that all types have the same total volume fraction of CNTs, that is,

$$V_{cnt} = \left[\frac{z}{h} + \frac{1}{2}\right]^{q} V_{tcnt} \tag{1}$$

3. Theoretical formulations

Rolling one time the graphene sheet becomes SWCNTs which look like a cylinder as shown in Figure 1. It is assumed that vibration produced on rotating CNT and this rotating tube length *L*,

height *h*, and radius *R*, which are treated as geometrical parameters. The geometrical representation of these parameters are shown in Figure 2.

The resultant and moment forces of rotating CNT are expressed as:

$$\left(N_{xx}, N_{\theta\theta}, N_{x\theta}\right) = \int_{\frac{-h}{2}}^{\frac{h}{2}} \left(\sigma_{xx}, \sigma_{\theta\theta}, \sigma_{x\theta}\right) dz, \quad \left(M_{xx}, M_{\theta\theta}, M_{x\theta}\right) = \int_{\frac{-h}{2}}^{\frac{h}{2}} \left(\sigma_{xx}, \sigma_{\theta\theta}, \sigma_{x\theta}\right) z dz \tag{2}$$

The stress components σ_{xx} (axial direction) and $\sigma_{\theta\theta}$ (tangential direction) and the stress vector $\sigma_{x\theta}$ in the $x\theta$-plane.

From Eq. (9), the elements of stress vector with the help of Hook's law can be elaborated as

$$\begin{pmatrix} \sigma_{xx} \\ \sigma_{\theta\theta} \\ \sigma_{x\theta} \end{pmatrix} = \begin{bmatrix} Q_{11} & Q_{12} & 0 \\ Q_{12} & Q_{22} & 0 \\ 0 & 0 & Q_{66} \end{bmatrix} \begin{pmatrix} e_{xx} \\ e_{\theta\theta} \\ e_{x\theta} \end{pmatrix} \tag{3}$$

Similarly the strain components (e_{xx}, $e_{\theta\theta}$) in x- and θ-directions whereas shear stress ($e_{x\theta}$) in the $x\,\theta$-plane.

The following form is for the strain energy (∇) of vibrating CNT

$$\nabla = \frac{1}{2} \int_0^L \int_0^{2\pi} [\beta]^T \left[\Gamma\right][\beta] R d\theta dx \tag{4}$$

where

$$[\beta]^T = \left[e_{11}, e_{22}, e_{12}, \kappa_{11}, \kappa_{22}, 2\kappa_{12}\right] \tag{5}$$

By utilizing the above matrices, the full form of $\left[\Gamma\right]$ is described as:

$$[\Gamma]=\begin{bmatrix} A_{11} & A_{12} & 0 & B_{11} & B_{12} & 0 \\ A_{12} & A_{22} & 0 & B_{12} & B_{22} & 0 \\ 0 & 0 & A_{66} & 0 & 0 & B_{66} \\ B_{11} & B_{12} & 0 & D_{11} & D_{12} & 0 \\ B_{12} & B_{22} & 0 & D_{12} & D_{22} & 0 \\ 0 & 0 & B_{66} & 0 & 0 & D_{66} \end{bmatrix} \tag{6}$$

The membrane, coupling, flexural rigidity are termed as (A_{ij}), (B_{ij}) and (D_{ij}), respectively.

$$[A_{ij}, B_{ij}, D_{ij}] = \int_{-h/2}^{h/2} Q_{ij}[1, z, z^2]dz, \tag{7}$$

For heterogeneous, the coupling stiffness B_{ij}'s, coupling stiffness eliminated for isotropic CNT. For laminated (isotropic) material, the reduced rigidity Q_{ij} with conjunction of Young's modulus and Poisson's ratio can be described as:

$$Q_{11} = \frac{E}{1-\nu^2} = Q_{22},\ Q_{12} = \frac{\nu E}{1-\nu^2},\ Q_{66} = \frac{E}{2(1+\nu)} \tag{8}$$

The parameter (E, ν, Q_{66}) used in Eq. (15) stands as Young's modulus, Poisson's ratio and shear modulus, respectively. A new theory is developed [18] with modification of Love's theory [17].

With the help of Love's theory[17], the linear combination of strain vector in Eq. (2) can be written as:

$$e_{xx} = e_{11} + z\kappa_{11},\ e_{\theta\theta} = e_{22} + z\kappa_{22},\ \ e_{x\theta} = e_{12} + 2z\kappa_{12} \tag{9}$$

whereas (κ_{11}, κ_{22}, κ_{12}) and (e_{11}, e_{22}, e_{12}) are referenced as surface curvatures and surface strains.

The interlinked relation of displacement functions (strain and curvature) is indicated as:

$$\left[e_{11}, e_{22}, \mathrm{e}_{12}\right] = \left[\frac{\partial u}{\partial x}, \frac{1}{R}\left(\frac{\partial v}{\partial \theta} + w\right), \left(\frac{\partial v}{\partial x} + \frac{1}{R}\frac{\partial u}{\partial \theta}\right)\right]$$

$$\left[\kappa_{11},\kappa_{22},\kappa_{12}\right]=\left[-\frac{\partial^2 w}{\partial x^2},-\frac{1}{R^2}\left(\frac{\partial^2 w}{\partial\theta^2}-\frac{\partial v}{\partial\theta}\right),-\frac{1}{R}\left(\frac{\partial^2 w}{\partial x\partial\theta}-\frac{\partial v}{\partial x}\right)\right] \tag{10}$$

The new form of strain energy is obtained after substituting Eqs. (5), (6) in Eq. (4).

$$\nabla=\frac{1}{2}\left(\begin{array}{l}\int_0^L\int_0^{2\pi} A_{11}{e_{11}}^2+A_{22}{e_{22}}^2+2A_{12}e_{11}e_{22}+A_{66}{e_{12}}^2+2B_{11}e_{11}\kappa_{11}+2B_{12}e_{11}\kappa_{22}+2B_{12}e_{22}\kappa_{11}\\ +2B_{22}e_{22}\kappa_{22}+4B_{66}e_{12}\kappa_{12}+D_{11}{\kappa_{11}}^2+D_{22}{\kappa_{22}}^2+2D_{12}\kappa_{11}\kappa_{22}+4D_{66}{\kappa_{12}}^2\end{array}\right)Rd\theta dx \tag{11}$$

The kinetic energy (K.E) of rotating tube is articulated as:

$$\Gamma=\frac{1}{2}\int_0^L\int_0^{2\pi}\left[\left(\frac{\partial u}{\partial t}\right)^2+\left(\frac{\partial v}{\partial t}+\Omega(R+w)\right)^2+\left(\frac{\partial w}{\partial t}-\Omega v\right)^2\right]R\rho_t d\theta dx \tag{12}$$

The mass density per unit length ρ_t is expressed as:

$$\rho_t=\int_{\frac{-h}{2}}^{\frac{h}{2}}\rho dz \tag{13}$$

where ρ designates the mass density.

The Lagrange energy functional ($\Im$) is expressed as the difference of strain and kinetic energies.

$$\Im=\Gamma-\nabla \tag{14}$$

After putting Eqs. (11 & 12) into Eq. (14) and by applying the Hamiltonian principle [50] to the Lagrange energy functional.

For executing the vibration of rotating CNTs, a set of partial PDEs containing displacement functions is developed as:

$$\frac{\partial N_{xx}}{\partial x}+\frac{1}{R}\frac{\partial N_{x\theta}}{\partial\theta}+\rho_t\Omega^2R^2\left(\frac{1}{R^2}\frac{\partial^2 u}{\partial\theta^2}-\frac{1}{R}\frac{\partial w}{\partial x}\right)=\rho_t\frac{\partial^2 u}{\partial t^2}$$

$$\frac{\partial N_{x\theta}}{\partial x}+\frac{1}{R}\frac{\partial N_{\theta\theta}}{\partial\theta}+\frac{1}{R}\frac{\partial M_{x\theta}}{\partial x}+\frac{1}{R^2}\frac{\partial M_{\theta\theta}}{\partial\theta}+\frac{\rho_t\Omega^2R^2}{R}\frac{\partial^2 u}{\partial x\partial\theta}-\rho_t\left(2\Omega\frac{\partial w}{\partial t}-\Omega^2 v\right)=\rho_t\frac{\partial^2 v}{\partial t^2}$$

$$\frac{\partial^2 M_{xx}}{\partial x^2}+\frac{2}{R}\frac{\partial^2 M_{x\theta}}{\partial x\partial\theta}+\frac{1}{R^2}\frac{\partial^2 M_{\theta\theta}}{\partial\theta^2}-\frac{N_{\theta\theta}}{R}+\frac{\rho_t\Omega^2R^2}{R^2}\left(\frac{\partial^2 w}{\partial\theta^2}-\frac{\partial v}{\partial\theta}\right)+\rho_t\left(2\Omega\frac{\partial v}{\partial t}+\Omega^2 w\right)=\rho_t\frac{\partial^2 w}{\partial t^2} \tag{15}$$

Utilizing the differential operator notations, Equation (15) forms a system of PDEs and these are calculated as:

$$\begin{aligned} d_{11}u + d_{12}v + d_{13}w &= \rho_t \frac{\partial^2 u}{\partial t^2} \\ d_{21}u + d_{22}v + d_{23}w &= \rho_t \frac{\partial^2 v}{\partial t^2} \\ d_{31}u + d_{32}v + d_{33}w &= \rho_t \frac{\partial^2 w}{\partial t^2} \end{aligned} \tag{15}$$

The mathematical expressions for these operators: $d_{11}, d_{12}, ..., d_{33}$ have been presented in Appendix 1.

3. 1 Application of Galerkin's method

Several techniques [78,79,80] have been proposed to analyze the vibration of CNT, but here, Galerkin's method to discretize the governing equation of motion. The coordinate system x, ϕ, t are designated for axial, circumferential and time variable and the following relations for displacement functions are stated as:

$$\begin{aligned} u(x,\theta,t) &= U(x)\alpha_m \cos(n\theta + \omega t) \\ v(x,\theta,t) &= V(x)\beta_m \sin(n\theta + \omega t) \\ w(x,\theta,t) &= W(x)\gamma_m (x-a)\cos(n\theta + \omega t) \end{aligned} \tag{16}$$

Where three vibrational amplitude coefficients ($\alpha_m, \beta_m, \gamma_m$) and the deformation [*u(x, θ, t), v(x, θ, t), w(x, θ, t)*] denotes, respectively, the axial, circumferential and radial direction. Here the axial deformation [$U(x), V(x), W(x)$] respectively, in the longitudinal, tangential and transverse direction. Here *m*, *n* are represented, respectively, the circumferential wave numbers, axial half and ω denoted by angular frequency. The formula of frequency is $f = \omega/2\pi$. In the tube vibration, $(x-a)$ treated as the impact of ring support and in this factor x designates axial variable and *a* is position of the ring support. We obtain following relation after putting Equation (16) in Equation (15) and replacing the operator expressions with integrating from $x = 0$ to $x = L$.

$$\left[-\frac{A_{12}}{R}\int_0^L (x-a)W(x)\frac{dU}{dx}dx + B_{11}\int_0^L (x-a)W(x)\frac{d^3U}{dx^3}dx - n^2\frac{(B_{12}+2B_{66})}{R^2}\int_0^L (x-a)W(x)\frac{dU}{dx}dx\right]\alpha_m$$

$$+\left[\begin{array}{l}\left(n(B_{12}+2B_{66})/R+\frac{(D_{12}+4D_{66})}{R^2}\right)\int_0^L (x-a)W(x)\frac{d^2V}{dx^2}dx + n\left(\frac{A_{22}}{R}+\frac{B_{22}}{R^3}-\rho_t\Omega^2\right)\int_0^L (x-a)W(x)V(x)dx + \\ n^3\left(\frac{B_{22}}{R^3}+\frac{D_{22}}{R^4}\right)\int_0^L (x-a)W(x)V(x)dx - 2\rho_t\Omega\omega\int_0^L (x-a)W(x)V(x)dx\end{array}\right]\beta m$$

$$-\left[\begin{array}{l}D_{11}\int_0^L (x-a)^2W(x)\frac{d^4W}{dx^4}dx + 4D_{11}\int_0^L (x-a)W(x)\frac{d^3W}{dx^3}dx + 2\frac{B_{12}}{R}\int_0^L (x-a)^2W(x)\frac{d^2W}{dx^2}dx + 4\frac{B_{12}}{R}\int_0^L (x-a)W(x)\frac{dW}{dx}dx \\ +n^2(\frac{2D_{12}+4D_{66}}{R^2})\int_0^L (x-a)^2W(x)\frac{d^2W}{dx^2}dx + 2n^2(\frac{2D_{12}+4D_{66}}{R^2})\int_0^L (x-a)W(x)\frac{dW}{dx}dx + n^2(\frac{2D_{12}+4D_{66}}{R^2})\int_0^L (x-a)W(x)\frac{d^2W}{dx^2}dx \\ +2n^2(\frac{2D_{12}+4D_{66}}{R^2})\int_0^L (x-a)W(x)\frac{dW}{dx}dx - n^4\frac{D_{22}}{R^4}\int_0^L (x-a)^2W^2(x)dx - n^2(2\frac{B_{22}}{R^3}+\rho_t\Omega^2)\int_0^L (x-a)^2W^2(x)dx \\ +(\rho_t\Omega^2-\frac{A_{22}}{R}+\rho_t\omega^2)\int_0^L (x-a)^2W^2(x)dx\end{array}\right]\gamma_m = 0 \quad (17)$$

The frequency matrix in the eigenvalue and polynomial form can be described after the arrangement of the above terms.

$$\left\{\begin{pmatrix}1&0&0\\0&1&0\\0&0&1\end{pmatrix}\rho_t\omega^2 + \begin{pmatrix}0&0&0\\0&0&1\\0&1&0\end{pmatrix}2\Omega\rho_t\omega + \begin{pmatrix}C_{11}&C_{12}&C_{13}\\C_{21}&C_{22}&C_{23}\\C_{31}&C_{32}&C_{33}\end{pmatrix}\right\}\begin{pmatrix}\alpha_m\\\beta_m\\\gamma_m\end{pmatrix} = 0 \quad (18)$$

or

$$\left\{L_1\omega^2 + L_2\omega + L_3\right\}[x] = 0 \quad (19)$$

Where the order of the matrix L_1, L_2, L_3 is three and the element of these matrices are presented in Appendix 2. Equation (19) be considered into standard eigenvalue problem w.r.t transformation [81].

$$\left(\begin{bmatrix}O&I\\-L_3&-L_2\end{bmatrix}\omega^2 - \begin{bmatrix}I&O\\O&L_1\end{bmatrix}\omega\right)\begin{Bmatrix}[x]\\\omega[x]\end{Bmatrix} = 0 \quad (20)$$

Where the order of O and I is three and specified as null and unit matrices.

Using MATLAB, the frequency of the tube consists of six values and for the tube stability minimum value has been chosen.

4. Results and discussions

In this section, the obtained results for the different BCs likewise: C-C and C-F for zigzag and chiral SWCNTs are parametrically studied in this part using proposed technique by Equation (20). Results reported in this study are verified with earlier theoretical/simulation. Here, the influence of boundary conditions (C-C & C-F) for zigzag and chiral tubes are performed. According to Galerkin's technique, the vibration frequencies have extended to wide range of parameters than earlier computations. In numerical simulation, the measurement of length-to-diameter ratio provides satisfactory results than those are obtained experimentally and numerically [18] for SWCNTs and the model demonstrates the ability to estimate the vibration behavior of SWCNTs. The computations of our newly model with proposed approach with same data sets, our results are consistent with previous reports in MD [18] for SWCNTs. The following material parameters are as, the ratio of Young's modulus and mass density, the in-plane stiffness or rigidity, Poisson's ratio E/ρ = 3.6481 × 10^8 m^2/s^2, Eh = 278.25 GPa·nm, ν = 0.2, respectively [18]. The range of poison's ratio and thickness of the tube is adjusted from ν = 0.14 ~ 0.34 and h = 0.0612 nm ~ 0.69 nm, respectively [42]and the diameter (d) of CNTs is considered as 6.86645×10^{-10} m.

Firstly, Frequencies are presented for non-rotating case along with non-dimensional frequency parameters as: $\chi = \omega R\sqrt{(1-\nu^2)\rho/E}$ shown in Tables 1 and 2 and good coherence is achieved. Tables 3 and 4 shows SWCNTs frequencies (THz) versus L/d. For the accuracy, the results are compared to the value estimated by wave propagation approach (WPA) [42] continuum model [19], (molecular dynamics) MD simulations [18], are given in Tables 3 and 4. The results are computed for wide range of L/d (= 4.68 ~13.89) with same parameters [18,19,42] The measurement of length-to-diameter ratio provides satisfactory results than those are obtained experimentally and numerically [18,19] and demonstrates the ability to estimate the vibration behavior of SWCNTs. The computations of our newly model with proposed approach and same data sets, our results are consistent with previous reports. The frequency difference is negligible

with the earlier computed results with different approaches. It is observed from two studies that molecular dynamic (MD) simulation have highest values than present results showing a frequency difference. Frequency spectra versus length/diameter ratio using Galerkin's method is determined with C-C and C-F end condition, found a satisfactory agreement. The schematic sketch of applied boundary conditions is shown in Figure 3 and details are given in Ref. [44].

The predicted current results are compared with the result predicted by Chen et al. [68] and percentage error is negligible in Table 5. The natural frequencies obtained using this formulation is in excellent agreement with other values reported in literature. The convergence shows that the present method is efficient and arising out of extensive mathematical manipulations and hence validating the formulation of rotating SWCNTs.

4.1 Frequency of rotating CNTs without ring supports

Firstly, rotating vibration frequency without ring supports of clamped-clamped CNTs are given in Tables 6–7, which denotes the frequency variation versus *L/R* and *h/R* for zigzag and chiral CNTs. During rotation, frequency waves bifurcate as backward and forward waves. When values of *L/R* enhanced, frequency decreases and become insignificant with parameter Ω =1rps q = 0.7, and *h/R* = 0.003, while on increasing *h/R*, frequency curves increases with specified parameter q = 0.7, Ω = 1rps, and *L/R* = 5. It is found that height-to-radius ratio is counter part of length-to-radius ratio. Table 8 demonstrates the variation of angular speed Ω (rps) versus frequency. The frequencies of backward waves increases and forward wave decreases on enhancing the angular speed with parameter *L/R* = 5, *h/R* = 0.003 and q = 0.7.

4.2 Frequency analysis of rotating CNTs with ring supports

In this section, we have obtained and discussed the variation of the vibrational frequency of length- and thickness-to-radius ratios under different nanotube boundary conditions. Moreover, the interpretation of lattice indices (m, n) can be formed as, for zigzag n = 0; and also chiral nanotubes as (m, n), for $n \neq m$ respectively. Here, vibration frequencies of zigzag (5, 0), (9, 0), and chiral (6, 4), (9, 5), SWCNTs, respectively have been performed using Galerkin's technique. Figures 4–5 shows the natural frequencies (Hz) for the backward and forward waves of rotating CNTs by varying ratio of length-to-radius, *L/R*. The other parameter for rotating shell are taken as Ω = 1rps, q = 0.7, *h/R* = 0.003 and a = 0.5. When the value of ratio *L/R* increases then

frequency decreases. The results for zigzag and chiral SWCNTs are investigated for ten computation with BCs (C-C and C-F) using Galerkin's method. The computed backward (forward) frequencies at *L/R* = 1 ~ 10 of zigzag (5, 0), (9, 0) are obtained as [93.104 (92.731) ~ 56.611 (56.242), 197.61 (197.4) ~ 190.48 (190.27)] for C-C conditions and [90.104 (90.031) ~ 54.61 (54.242), 195.61 (195.4) ~ 187.48 (187.27)] for C-F conditions as shown in Fig-4. Now frequencies for chiral tube index (6, 4), (9, 5) with above defined *L/R* are as [1248.35 (1248.31) ~ 163.61(163.16), 2088.89 (2088.67) ~239.46 (239.22)] and for C-F conditions [1148.35 (1148.31) ~ 63.611 (63.162), 1588.89 (1588.67) ~ 98.461 (88.299)] shown in Figure 5. These figures show that on enhancing the ratio *L/R*, the frequencies for zigzag and chiral cases decreases very fast. It is observed that values of zigzag frequency with specified boundary conditions are less than that of chiral frequency outcomes. As it is noted that the deformation is not easy in the chiral and zigzag tube. Moreover, the cross sectional deformation of chiral is greater than the zigzag. Due to this the fundamental frequencies of zigzag are less than the chiral tubes frequencies. Obviously, the frequency peaks of C-C are greater than C-F curves of SWCNTs.

Figures 6 – 7 show the effect of frequency response of isotropic zigzag and chiral against ratio of thickness-to-radius with proposed boundary conditions and other referenced parameter are remained constant. The numerical traceable frequencies of backward (forward) succeeding to *h/R* = 0.001 for end condition are C-C = (5, 0) *f* ~6.2815 (5.9142), (9, 0) *f* ~19.67 (19.461), (7, 6) *f* ~79.589 (79.133), (11, 4) *f* ~131.99 (131.62), and for end condition C-F = (5, 0) *f* ~3.2815 (2.9142), (9, 0) *f* ~17.67 (17.461), (7, 6) *f* ~58.589 (58.133), (11, 4) *f* ~121.99 (121.62) respectively. The natural frequencies at *h/R* = 0.010 for C-C = (5, 0) *f* ~56.791 (56.424), (9, 0) *f* ~191.19 (190.98), (6, 4) *f* ~88.653 (88.198), (9, 5) *f* ~150.59 (150.22), and for end condition C-F = (5, 0) *f* ~53.791 (53.424), (9, 0) *f* ~189.19 (189.98),(6, 4) *f* ~67.653 (67.198), (9, 5) *f* ~140.59 (140.22) as shown in Figures 6-7. From the above discussion, it can be perceived that on varying the *h/R*, the C-F frequencies (5, 0), (9, 0), (6, 4), (9, 5) are lower than that of C-C same indices. When *h/R* enhanced from 0.001 ~ 0.010 the frequency peaks are observed as pronounce and parallel. Vibration characteristics of rotating isotropic zigzag and chiral C-C and C-F SWCNT structure are performed in detail through current study. The fundamental frequencies of CNT versus rotating speed (Ω) as shown in Figures 8–9. The convergence is achieved of the presented Galerkin's technique results with the estimated values of Chen et al.[68.] Moreover, C-C

FNFs at Ω = 1, the backward (forward) waves are f ~[(5, 0), (9, 0)] 16.690 (16.521), 54.553 (54.390) and f (Hz)~[(6, 4), (9, 5)] 46.657 (46.506), 65.869 (65.778) and backward (forward) C-F FNFs are f ~[(5, 0), (9, 0)] 15.533 (15.411), 54.635 (54.445) and f (Hz)~[(6, 4), (9, 5)] 45.657(45.506), 64.869 (64.778). The frequency of backward (forward) C-C FNFs at Ω = 9 are f (Hz)~[(5, 0), (9, 0)] 18.338(14.998), 57.321 (53.998) and f (Hz)~[(6, 4), (9, 5)]), 47.55(46.188), 66.935 (65.602) and backward (forward) C-F FNFs are f (Hz)~[(5, 0), (9, 0)] 17.338(13.998), 56.321 (52.998) and f (Hz)~[(6, 4), (9, 5)] 46.55 (45.188), 65.935 (64.602).

Further, it is remarkable from Figures 8–9, that the isotropic rotating frequency curves of chiral SWCNTs are definitely greater than that of zigzag curves. For backward and forward waves, it can be seen that the frequency amplitudes of both types of SWCNTs remain same at Ω = 0. The frequency curves of forward waves are slightly less than forward waves validating the earlier computation [12,78] The presented Galerkin's technique for backward and forward waves of these tubes provides higher estimation definitely for whole range of Ω. It is noted that from the figures on increasing the rotational speed, the backward waves monotonically increases and forward waves decreases, respectively for C-C and C-F.

Figures 10–11 presents the backward and forward frequencies (Hz) for two types of CNTs versus the positions of ring supports (a). The remaining referenced parameters are Ω = 1rps L/R = 5, h/R = 0.003 and q = 0.7. The ring support is composed as $(0 \le a \le L)$. The frequency results of backward (forward) for C-C at a = 0 are [f ~ (5, 0), (9, 5)] 414.74 (414.68),674.64 (676.61) and at $a = 0.5L$ [f ~ (9, 0), (9, 5)] 588.42 (588.21),900.1 (900.1) and $a = L$ [f ~ (8, 0), (9, 5)]414.74 (414.68),674.64 (676.61). The frequency outcomes of C-F backward (forward) at a = 0 are [f ~ (8, 0), (9, 5)] 366.74 (366.68),659.64 (659.61) and at $a = 0.5L$ [f ~ (8, 0), (9, 5)] 540.42 (540.21),890.65 (890.45) and $a = L$ [f ~ (8, 0), (9, 5)] 366.74 (366.68),659.64 (659.61).
On increasing the ring positions, the frequencies increases from a = 0 ~0.4 and attains maximum values at a = 0.5L and after a = 0.5L the frequencies decreases. The frequency has same value at ring position a = 0, 1. It is evident from the figures that when the values of a $(0 \le a \le L)$ increases then the natural frequencies also increases and $a = 0.5L$, it reaches its peak value but for $0.5L < a < L$, on increasing the value of a, it begins to decrease and rust itself as bell shape symmetric curve. The same trend is observed for the other zigzag and chiral indices. It is seen

that effect of ring support is highly prominent on the vibration of rotating isotropic CNTs. The frequency values enhance on locating the ring supports around the rotating CNTs.

5. Conclusions

In this section, a comprehensive estimation regarding Love's shell theory has been considered for vibrational behavior of the rotating isotropic SWCNTs with distinct parameters using Galerkin's method. Vibration frequency spectra of various physical parameters such as length-to-radius ratios angular speed and height-to-radius ratios, have been obtained with the effects ring supports for the vibrational behavior of different zigzag and chiral SWCNTs. Also the effects of ring supports have been originally examined for these types of tubes. Due to rotation of the tube, the frequency curves bifurcate as backward and forward frequencies. It has been demonstrated that the fundamental natural frequencies (backward and forward) depend on the material parameters of the nanotube and the frequencies for two sorts of SWCNTs under C-C and C-F boundary conditions increase with the decrease of length-to-radius ratio. In addition, it was indicated that the natural frequencies of these tubes increases with the increase of height-to-radius ratio. Throughout the computation from this model, the frequencies of C-C conditions are larger than C-F, due to constraints are applied at the end of the tube. It is also found that on enhancing the position of the ring supports, the frequency curves increase in the start and at the mid are higher and at the last the frequencies are same as the frequencies was observed in the start of attached ring supports. It is concluded that ring supports have great effect on the frequencies of zigzag and chiral tubes. The present work can be utilized for analyzing of the vibrations in carbon nanotube by considering different parameters, namely, Winkler and Pasternak foundations, geometrical imperfections, fluid conveying, thermal and electromagnetic effects.

Declaration of Conflicting Interests

The author(s) declared no potential conflicts of interest with respect to the research, authorship, and/or publication of this article.

Funding

The author(s) received no financial support for the research, authorship, and/or publication of this article.

ORCID iD

Muzamal Hussain http://orcid.org/0000-0002-6226-359X

References

1. Iijima S. Helical microtubules of graphitic carbon. *Nature* 1991;354:56–58.
2. Subramanian A, Oden P.I, Kennel S.J, Jacobson K.B, Warmack R.J, Thundat T, Doktycz M.J. Glucose biosensing using an enzyme-coated microcantilever. *Applied Physics Letters* 2002;81:385–387.
3. Li M, Tang HX, Roukes M.L. Ultra-sensitive NEMS-based cantilevers for sensing, scanned probe and very high-frequency applications. *Nature Nanotechnology* 2007;2: 114–120.
4. Chun DK and Bert CW. Critical speed analysis of laminated composite. *Hollowdrive shafts. Compos. Eng.* 1993; 3: 633–643.
5. Torkaman-Asadi MA, Rahmanian M and Firouz-Abadi RD. Free vibrations and stability of high-speed rotating carbon nanotubes partially resting on Winkler foundations. *Composite Structures* 2015;126:52-61.
6. Eltaher MA, Emam SA and Mahmoud FF. Free vibration analysis of functionally graded size-dependent nanobeams. *Appl. Math. Comput.* 2012; 218: 7406–7420.
7. Arshad SH, Naeem MN and Sultana N. Frequency analysis of functionally graded cylindrical shells with various volume fraction laws. *Journal of Mechanical Engineering Science* 2007; 221(C): 1483–1495.
8. Ansari R and Darvizeh M. Prediction of dynamic behavior of FGM shells under arbitrary boundary conditions. *Composite Structures* 2008; 85(4): 284–292.
9. Malekzadeh P and Heydarpour Y. Free vibration analysis of rotating functionally graded cylindrical shells in thermal environment. *Composite Structures* 2012; 94: 2971–2981
10. Koizumi M. FGM Activities in Japan, *Composites* 1997.
11. Yamanouchi M, Koizumi M, Hirai T and Shiota I. FGM-90. *In Proceedings of the First International Symposium on Functionally Gradient Materials* FGM Forum, Tokyo, Japan 1990.
12. Hussain M, Naeem MN and Isvandzibaei MR. Effect of Winkler and Pasternak elastic foundation on the vibration of rotating functionally graded material cylindrical

shell. *Proceedings of the Institution of Mechanical Engineers, Part C: Journal of Mechanical Engineering Science* 2018, 0954406217753459.

13. Swaddiwudhipong S, Tian J and Wang CM. Vibration of cylindrical shells with ring supports. *J Sound and Vibration* 1995; 187(1): 69–93.
14. Hussain M, Naeem MN, Shahzad A, and He M. Vibration characteristics of fluid-filled functionally graded cylindrical material with ring supports. Chapter, *Computational Fluid Dynamics* 2018, ISBN 978-953-51-5706-9, DOI: 10.5772/intechopen.72172.
15. Love, AEH. A treatise on the mathematical theory of elasticity. 4th Edn, *Cambridge* 1952.
16. Budiansky B and Sanders JL. On the best first order linear shell theory, *progress in applied mechanics*. *MacMillan, Inc., Greenwich, Conn.* 1963; 192: 129–140.
17. Markûs S. The mechanics of vibrations of cylindrical shells. *Elsevier, Amsterdam* 1988.
18. Zhang YY, Wang CM and Tan VBC. Assessment of Timoshenko beam models for vibrational behavior of single-walled carbon nanotubes using molecular dynamics. *Adv. Appl. Math. Mech.* 2009; 1(1): 89–106.
19. Wang CM, Ma YQ, Zhang YY and Ang KK. Buckling of double-walled carbon nanotubes modeled by solid shell elements. *Journal of applied physics* 2006; 99(11): 114317.
20. Bocko J and Lengvarský P. Vibration of single-walled carbon nanotubes by using nonlocal theory. *American Journal of Mechanical Engineering* 2014; 2: 195–198.
21. Swain A, Roy T and Nanda BK. Vibration behavior of single-walled carbon nanotube using finite element. *Int. J. Theor. And Appl. Res. in Mech. Eng.* 2013; 2: 129–133.
22. Fernandes R, El-Borgi S, Mousavi SM, Reddy, JN, Mechmoum A. Nonlinear size-dependent longitudinal vibration of carbon nanotubes embedded in an elastic medium. *Physica E: Low-dimensional Systems and Nanostructures* 2017; 88, 18–25.
23. Trabelssi M, El-Borgi S, Ke LL, Reddy, JN. Nonlocal free vibration of graded nanobeams resting on a nonlinear elastic foundation using DQM and La DQM. *Composite Structures* 2017; 176: 736–747.
24. Goncalves BR, Karttunen A, Romanoff J and Reddy JN. Buckling and free vibration of shear-flexible sandwich beams using a couple-stress-based finite element. *Composite Structures* 2017; 165: 233–241.

25. Kim J, Żur, KK., and Reddy JN. Bending, free vibration, and buckling of modified couples stress-based functionally graded porous micro-plates. *Composite Structures* 2019; 209: 879–888.
26. Bellifa H, Benrahou KH, Bousahla AA, Tounsi A and Mahmoud SR. A nonlocal zeroth-order shear deformation theory for nonlinear postbuckling of nanobeams. *Structural Engineering and Mechanics* 2017; 62(6): 695–702.
27. Youcef DO, Kaci A, Benzair A, Bousahla AA, and Tounsi A. Dynamic analysis of nanoscale beams including surface stress effects. Smart structures and systems, 2018; 21(1): 65-74.
28. Hamza-Cherif R, Meradjah, M, Zidour M, Tounsi A, Belmahi S, and Bensattalah, T. Vibration analysis of nano beam using differential transform method including thermal effect. *Journal of Nano Research, Trans Tech Publications* 2018; 54: 1–14.
29. Chaht FL, Kaci A, Houari MSA, Tounsi A, Bég OA, and Mahmoud SR. Bending and buckling analyses of functionally graded material (FGM) size-dependent nanoscale beams including the thickness stretching effect. *Steel and Composite Structures* 2015; 18(2): 425–442.
30. Kadari B, Bessaim A, Tounsi A, Heireche H, Bousahla AA, and Houari MSA. Buckling analysis of orthotropic nanoscale plates resting on elastic foundations. *Journal of Nano Research; Trans Tech Publications* 2018; 55: 42–56.
31. Karami B, Janghorban M, and Tounsi A. Effects of triaxial magnetic field on the anisotropic nanoplates. *Steel and composite structures* 2017; 25(3): 361–374.
32. Yazid M, Heireche H, Tounsi A, Bousahla AA and Houari MSA. A novel nonlocal refined plate theory for stability response of orthotropic single-layer graphene sheet resting on elastic medium. *Smart structures and systems* 2018; 21(1): 15–25.
33. Karami B, Janghorban M, and Tounsi A. Nonlocal strain gradient 3D elasticity theory for anisotropic spherical nanoparticles. *Steel and composite structures* 2018; 27(2): 201-216.
34. Mouffoki A, Bedia EA, Houari MSA, Tounsi A, and Mahmoud SR. Vibration analysis of nonlocal advanced nanobeams in hygro-thermal environment using a new two-unknown trigonometric shear deformation beam theory. *Smart Structures and Systems* 2017, 20(3), 369–383.

35. Wuite J and Adali S. Deflection and stress behavior of nanocomposite reinforced beams using a multiscale analysis. *Composite Structures* 2005; 71(3–4), 388–396.
36. Bouafia K, Kaci A, Houari MSA, Benzair A, and Tounsi A. A nonlocal quasi-3D theory for bending and free flexural vibration behaviors of functionally graded nanobeams. *Smart Structures and Systems* 2017, 19(2): 115–126.
37. Bounouara F, Benrahou KH, Belkorissat I, and Tounsi A. A nonlocal zeroth-order shear deformation theory for free vibration of functionally graded nanoscale plates resting on elastic foundation. *Steel and Composite Structures* 2016; 20(2): 227–249.
38. Ebrahimi F, Jafari A, and Barati MR. Vibration analysis of magneto-electro-elastic heterogeneous porous material plates resting on elastic foundations. *Thin-Walled Structures* 2017; 119: 33–46.
39. Zemri A, Houari MSA, Bousahla AA, and Tounsi A. A mechanical response of functionally graded nanoscale beam: an assessment of a refined nonlocal shear deformation theory beam theory. *Structural engineering and mechanics* 2015; 54(4), 693–710.
40. Ahouel M, Houari MSA, Bedia EA, and Tounsi A. Size-dependent mechanical behavior of functionally graded trigonometric shear deformable nanobeams including neutral surface position concept. *Steel and Composite Structures* 2016; 20(5): 963–981.
41. Gao K, Gao W, Chen D and Yang J. Nonlinear free vibration of functionally graded graphene platelets reinforced porous nanocomposite plates resting on elastic foundation. *Composite Structures* 2018; 204: 831–846.
42. Hussain M, Naeem MN, Shahzad A and He M. Vibrational behavior of single-walled carbon nanotubes based on cylindrical shell model using wave propagation approach. *AIP Advances* 2017; 7(4): 045114.
43. Zhou K, Huang X, Tian J and Hua H. Vibration and flutter analysis of supersonic porous functionally graded material plates with temperature gradient and resting on elastic foundation. *Composite Structures* 2018; 204: 63–79.
44. Hussain M and Naeem MN. Vibration analysis of single-walled carbon nanotubes using wave propagation approach. *Mechanical Sciences* 2017; 8(1): 155–164.
45. Hussain M and Naeem MN. Vibration of single-walled carbon nanotubes based on Donnell shell theory using wave propagation approach. Chapter, *Intechopen*, *Novel*

Nanomaterials - Synthesis and Applications 2018, ISBN 978-953-51-5896-7,10.5772/intechopen.73503.

46. Żur KK. Free vibration analysis of elastically supported functionally graded annular plates via quasi-Green's function method. *Composites Part B: Engineering* 2018; 144: 37–55.
47. Besseghier A, Houari MSA, Tounsi A, and Mahmoud SR. Free vibration analysis of embedded nanosize FG plates using a new nonlocal trigonometric shear deformation theory. *Smart Structures and Systems* 2017; 19(6): 601–614.
48. Khetir H, Bouiadjra MB, Houari MSA, Tounsi A, and Mahmoud SR. A new nonlocal trigonometric shear deformation theory for thermal buckling analysis of embedded nanosize FG plates. *Structural Engineering and Mechanics* 2017; 64(4), 391–402.
49. Belkorissat I, Houari MSA, Tounsi A, Bedia EA, and Mahmoud SR On vibration properties of functionally graded nano-plate using a new nonlocal refined four variable model. *Steel Compos. Struct* 2015; 18(4): 1063–1081.
50. Mokhtar Y, Heireche H, Bousahla AA, Houari MSA, Tounsi A, and Mahmoud SR. A novel shear deformation theory for buckling analysis of single layer graphene sheet based on nonlocal elasticity theory. *Smart structures and systems* 2018; 21(4): 397–405.
51. Bouadi A, Bousahla AA, Houari MSA, Heireche H, and Tounsi A. A new nonlocal HSDT for analysis of stability of single layer graphene sheet. *Advances in Nano Research* 2018; 6(2): 147–162.
52. Karami B, Janghorban M and Tounsi A. Variational approach for wave dispersion in anisotropic doubly-curved nanoshells based on a new nonlocal strain gradient higher order shell theory. *Thin-Walled Structures* 2018; 129: 251–264.
53. Bakhadda B, Bouiadjra MB, Bourada F, Bousahla AA, Tounsi A, and Mahmoud SR. Dynamic and bending analysis of carbon nanotube-reinforced composite plates with elastic foundation. *Wind and Structures* 2018; 27(5): 311–324.
54. Pradhan SC and Phadikar J K. Nonlocal elasticity theory for vibration of nanoplates. *Journal of Sound and Vibration* 2009;325(1-2):206-223.
55. Shen HS. Nonlinear bending of functionally graded carbon nanotube-reinforced composite plates in thermal environments. *Composite Structures* 2009; 91(1): 9–19.

56. Ke, LL, Yang J and Kitipornchai S. Nonlinear free vibration of functionally graded carbon nanotube-reinforced composite beams. *Composite Structures* 2010; 92(3): 676–683.
57. Wang ZX and Shen HS. Nonlinear vibration of nanotube-reinforced composite plates in thermal environments. *Computational Materials Science* 2011; 50(8): 2319–2330.
58. Wang ZX and Shen HS. Nonlinear vibration and bending of sandwich plates with nanotube-reinforced composite face sheets. *Composites Part B-Engineering* 2012; 43(2): 411–421.
59. Shen HS and Xiang Y. Nonlinear vibration of nanotube-reinforced composite cylindrical shells in thermal environments. *Computer Methods in Applied Mechanics and Engineering* 2012; 213*:* 196–205.
60. Aragh BS, Barati AHN, and Hedayati H. Eshelby-Mori-Tanaka approach for vibrational behavior of continuously graded carbon nanotube-reinforced cylindrical panels. *Composites Part B-Engineering* 2012; 43(4): 1943–1954.
61. Żur KK. Quasi-Green's function approach to free vibration analysis of elastically supported functionally graded circular plates. *Composite Structures* 2018; 183: 600-610.
62. Rafiee M, Yang J and Kitipornchai S. Large amplitude vibration of carbon nanotube reinforced functionally graded composite beams with piezoelectric layers. *Composite Structures* 2013; 96: 716–725.
63. Wattanasakulpong N and Ungbhakorn V. Analytical solutions for bending, buckling and vibration responses of carbon nanotube-reinforced composite beams resting on elastic foundation. *Computational Materials Science* 2013; 71*:* 201–208.
64. Shahsavari D, Shahsavari M, Li L, & Karami B. A novel quasi-3D hyperbolic theory for free vibration of FG plates with porosities resting on Winkler/Pasternak/Kerr foundation. *Aerospace Science and Technology* 2018; 72: 134–149.
65. Murmu T and Adhikari S. Scale-dependent vibration analysis of prestressed carbon nanotubes undergoing rotation. *J Appl Phys* 2010; 108: 123507.
66. Naeem MN. Prediction of natural frequencies for functionally graded cylindrical shells. Ph.D. Thesis, UMIST, UK (2004).
67. Naeem MN, Iqbal Z. Sultana N. Vibration characteristics of FGM circular cylindrical shells using wave propagation approach. *Acta Mech* 2009; 208: 237–248.

68. Chen Y, Zhao HB and Shea ZP. Vibrations of high speed rotating shells with calculations for cylindrical shells. *Journal of Sound and Vibration* 1993; 160: 137–160.
69. Ahmad M and Naeem MN. Vibration characteristics of rotating FGM circular cylindrical shell using wave propagation method. *European Journal of Scientific Research*, 2009; 36(2): 184–235.
70. Heydarpour Y, Aghdam MM and Malekzadeh P. Free vibration analysis of rotating functionally graded carbon nanotube-reinforced composite truncated conical shells *Composite Structures* 2014; 117: 187–200.
71. Mirzaei M and Kiani Y. Free vibration of functionally graded carbon-nanotube-reinforced composite plates with cutout. *Beilstein journal of nanotechnology* 2016; 7: 511.
72. Nguyen Dinh D and Nguyen PD. The dynamic response and vibration of functionally graded carbon nanotube-reinforced composite (FG-CNTRC) truncated conical shells resting on elastic foundations. *Materials* 2017; 10(10): 1194.
73. Thomas B and Roy T. Vibration and damping analysis of functionally graded carbon nanotubes reinforced hybrid composite shell structures. *Journal of Vibration and Control* 2017; 23(11): 1711–1738.
74. Javaheri R and Eslami MR. Thermal buckling of functionally graded plates based on higher order theory. *Journal of thermal stresses* 2003; 25(7): 603–625.
75. Shen HS. Postbuckling of nanotube-reinforced composite cylindrical shells in thermal environments. *Part I: Axially-loaded shells. Composite Structures* 2011; 93(8): 2096-2108.
76. Jam JE and Kiani Y. Buckling of pressurized functionally graded carbon nanotube reinforced conical shells. *Composite Structures* 2015; 125: 586-595.
77. Sodel W. Vibration of shell and plates. *Mechanical engineering series*, Marcel Dekker, New York 1981.
78. Hussain M, Naeem MN, Shahzad A, He M and Habib S. Vibrations of rotating cylindrical shells with FGM using wave propagation approach. *Part C: Journal of Mechanical Engineering Science* 2018; 232(23):4342–4356.

79. Hussain M and Naeem MN. Effect of various edge conditions on free vibration characteristics of rectangular plates, Chapter, *Advance Testing and Engineering*, ISBN 978-953-51-6706-8, 2018.
80. Hussain M and Naeem MN. Vibration characteristics of single-walled carbon nanotubes based on non-local elasticity theory using wave propagation approach (WPA) including chirality. Chapter, *Carbon nanotubes*, ISBN 978-1-78984-402-3, 2019.
81. Dong SB. A block-stodola eigen solution technique for large algebraic systems with non-symmetrical matrices. *International Journal of Numerical Methods in Engineering* 1977; 11: 247.

Appendices

Appendix 1

$$d_{11} = A_{11}\frac{\partial^2}{\partial x^2} + \left(\frac{A_{66}}{R^2} + \rho_t\Omega^2\right)\frac{\partial^2}{\partial\theta^2}$$

$$d_{12} = \frac{\left(A_{12}+A_{66}\right)}{R}\frac{\partial^2}{\partial x\partial\theta} + \frac{\left(B_{12}+2B_{66}\right)}{R^2}\frac{\partial^2}{\partial x\partial\theta}$$

$$d_{13} = \left(\frac{A_{12}}{R} - \rho_t\Omega^2 R\right)\frac{\partial}{\partial x} - B_{11}\frac{\partial^3}{\partial x^3} - \frac{\left(B_{12}+2B_{66}\right)}{R^2}\frac{\partial^3}{\partial x\partial\theta^2}$$

$$d_{21} = \left(\frac{A_{12}+A_{66}}{R} + \frac{B_{12}+B_{66}}{R^2} + \rho_t\Omega^2 R\right)\frac{\partial^2}{\partial x\partial\theta}$$

$$d_{22} = \left(A_{66} + \frac{3B_{66}}{R} + \frac{2D_{66}}{R^2}\right)\frac{\partial^2}{\partial x^2} + \left(\frac{A_{22}}{R^2} + \frac{2B_{22}}{R^3} + \frac{D_{22}}{R^4}\right)\frac{\partial^2}{\partial\theta^2} + \rho_t\Omega^2$$

$$d_{23} = \left(\frac{A_{22}}{R^2} + \frac{B_{22}}{R^3}\right)\frac{\partial}{\partial\theta} - \left(\frac{B_{22}}{R^3} + \frac{D_{22}}{R^4}\right)\frac{\partial^3}{\partial\theta^3} - \left(\frac{B_{12}+2B_{66}}{R} + \frac{D_{12}+2D_{66}}{R^2}\right)\frac{\partial^3}{\partial x^2\partial\theta} - 2\rho_t\Omega\frac{\partial}{\partial t}$$

$$d_{31} = -\frac{A_{12}}{R}\frac{\partial}{\partial x} + B_{11}\frac{\partial^3}{\partial x^3} + \left(\frac{B_{12}+2B_{66}}{R^2}\right)\frac{\partial^3}{\partial x\partial\theta^2}$$

$$d_{32} = -\left(\frac{A_{22}}{R^2} + \frac{B_{22}}{R^3} + \rho_t\Omega^2\right)\frac{\partial}{\partial\theta} + \left(\frac{B_{22}}{R^3} + \frac{D_{22}}{R^4}\right)\frac{\partial^3}{\partial\theta^3} + \left(\frac{B_{12}+2B_{66}}{R} + \frac{D_{12}+4D_{66}}{R^2}\right)\frac{\partial^3}{\partial x^2\partial\theta} + 2\rho_t\Omega\frac{\partial}{\partial t}$$

$$d_{33} = -\frac{A_{22}}{R^2} + \rho_t\Omega^2 + \frac{2B_{12}}{R}\frac{\partial^2}{\partial x^2} + \left(\frac{2B_{22}}{R^3} + \rho_t\Omega^2\right)\frac{\partial^2}{\partial\theta^2} - D_{11}\frac{\partial^4}{\partial x^4} - 2\left(\frac{D_{12}+2D_{66}}{R^2}\right)\frac{\partial^4}{\partial x^2\partial\theta^2} - \frac{D_{22}}{R^4}\frac{\partial^4}{\partial\theta^4}$$

Appendix 2

$$C_{11} = A_{11} I_1 - n^2 \left[\frac{A_{66}}{R^2} + \rho_t \Omega^2 \right] I_2$$

$$C_{12} = -n \left[\frac{A_{12} + A_{66}}{R} \right] I_2 - n \left[\frac{B_{12} + 2B_{66}}{R^2} \right] I_2$$

$$C_{13} = \left[\frac{A_{12}}{R} - \rho_t \Omega^2 R \right] I_4 - B_{11} I_5 + n^2 \left[\frac{B_{12} + 2B_{66}}{R^2} \right] I_4$$

$$C_{21} = n \left[\frac{A_{12} + A_{66}}{R} \right] I_5 + \rho_t \Omega^2 R I_5 + \left[\frac{B_{12} + B_{66}}{R^2} \right] I_6$$

$$C_{22} = \left[\frac{A_{66} + 2D_{66}}{R^2} + \frac{3B_{66}}{R} \right] I_7 - n^2 \left[\frac{A_{22}}{R} + \frac{D_{22}}{R^4} \right] I_8 + \rho_t \Omega^2 I_8 + 2n^2 \frac{B_{22}}{R^3} I_8$$

$$C_{23} = n \left[\frac{A_{22}}{R} + \frac{B_{22}}{R^3} \right] I_9 - n \left[\frac{B_{12} + 2B_{66}}{R} \right] I_9 + \left[\frac{D_{12} + 2D_{66}}{R^2} \right] I_{10} + n^3 \left[\frac{B_{22}}{R^3} + \frac{D_{22}}{R^4} \right] I_9$$

$$C_{31} = -\frac{A_{12}}{R} I_{11} + B_{11} I_{12} - n^2 \left[\frac{B_{12} + 2B_{66}}{R^2} \right] I_{11}$$

$$C_{32} = -n \left[\frac{D_{12} + 4D_{66}}{R^2} \right] I_{13} + n \left[\frac{A_{22}}{R} - \rho_t \Omega^2 \right] I_{14} + n^3 \frac{D_{22}}{R^4} I_{14} - n \left[\frac{B_{12} + 2B_{66}}{R} \right] I_{13} + n^3 \frac{B_{22}}{R^3} I_{14} + n \frac{B_{22}}{R^3} I_{14}$$

$$C_{33} = -D_{11} I_{15} + n^2 \left[\frac{2D_{12} + 4D_{66}}{R^2} \right] I_{16} + 2 \frac{B_{12}}{R} I_{16} - n^4 \frac{D_{22}}{R^4} I_{17} - n^2 \left[\frac{2B_{22}}{R^3} + \rho_t \Omega^2 \right] I_{17} + \left[\rho_t \Omega^2 - \frac{A_{22}}{R} \right] I_{17}$$

where

$$I_1 = \int_0^L \frac{d^2 U}{dx^2} U(x) dx$$

$$I_2 = \int_0^L U(x) U(x) dx$$

$$I_3 = \int_0^L x \frac{dW}{dx} U(x) dx - a \int_0^L \frac{dW}{dx} U(x) dx + \int_0^L W(x) U(x) dx$$

$$I_4 = \int_0^L x \frac{d^3 W}{dx^3} U(x) dx - a \int_0^L \frac{d^3 W}{dx^3} U(x) dx + 3 \int_0^L \frac{d^2 W}{dx^2} U(x) dx$$

$$I_5 = \int_0^L \frac{dU}{dx} V(x)dx$$

$$I_6 = \int_0^L V(x)V(x)dx$$

$$I_7 = \int_0^L xW(x)V(x)dx - a\int_0^L W(x)V(x)dx$$

$$I_8 = \int_0^L x\frac{d^2W}{dx^2}V(x)dx - a\int_0^L \frac{d^2W}{dx^2}V(x)dx + 2\int_0^L \frac{dW}{dx}V(x)dx$$

$$I_9 = \int_0^L x\frac{dU}{dx}W(x)dx - a\int_0^L \frac{dU}{dx}W(x)dx$$

$$I_{10} = \int_0^L x\frac{d^3U}{dx^3}W(x)dx - a\int_0^L \frac{d^3U}{dx^3}W(x)dx$$

$$I_{11} = \int_0^L (x-a)^2 \frac{d^4W}{dx^4}W(x)dx + 4\int_0^L (x-a)\frac{d^3W}{dx^3}W(x)dx$$

$$I_{12} = \int_0^L (x-a)^2 \frac{d^2W}{dx^2}W(x)dx + 2\int_0^L (x-a)\frac{dW}{dx}W(x)dx$$

$$I_{13} = \int_0^L (x-a)^2 W(x)W(x)dx$$

$$I_{14} = \int_0^L (x-a)W(x)V(x)dx$$

$$I_{15} = \int_0^L (x-a)W(x)\frac{d^3W}{dx^3}dx$$

$$I_{16} = \int_0^L (x-a)W(x)\frac{dW}{dx}dx$$

$$I_{17} = \int_0^L (x-a)^2 W^2(x)dx$$

Notation

a	ring support	$u(x, \theta, t), v(x, \theta, t)$,	
E	Young's modulus	$w(x, \theta, t)$	deformed functions
E, ν, ρ	material parameters	ρ	density
f	fundamental frequency	$\alpha_m, \beta_m, \gamma_m$	vibration amplitude coefficients
h	tube thickness		
L	length of tube	Ω	angular speed
L/R , h/R	ratio of length and thickness-to-radius	ν	Poisson's ratio
		χ_b, χ_f	backward and forward frequency
m	half- axial wave number		
n	circumferential wave number	ω	angular frequency
q	exponent of volume fraction	θ	circumferential coordinate
R	tube radius		

Table 1. Comparison of SWCNT frequencies with Ref.[13].

L/R	*m*	Method	*n*			
			1	2	3	4
20	1	Swaddiwudhipong et al.[13]	0.016101	0.00545	0.00504	0.008534
		Present	0.016103	0.00545	0.00505	0.008536
0.25	1	Swaddiwudhipong et al.[13]	0.95193	0.93446	0.90673	0.87076
		Present	0.95194	0.93446	0.90674	0.87078

Table 2. Comparison of simply supported SWCNT natural frequencies with Ref.[69].

n	Method	1	2	3	4	5
2	Ahmad and Naeem [69]	2043.7	5635.3	8932.4	11407.4	13253.1
	Present	2046.4	5637.2	8933.4	11407.8	13253.0
3	Ahmad and Naeem[69]	2195.05	4035.55	6614.63	9121.1	11358.9
	Present	2199.03	4041.30	6619.2	9124.1	11360.8

Table 3. Comparison of mode (*m*, *n*) = (1, 1) C-C SWCNTs frequencies.

	Frequencies (THz)			
L/d	Present	WPA[42]	MD Simulation[18]	Shell model [19]
4.68	0.99714	1.23445	1.06812	1.1747
6.67	0.54244	0.67832	0.64697	0.5909
8.47	0.35204	0.44146	0.43335	0.4625
10.26	0.24696	0.30922	0.30518	0.3494
13.89	0.13814	0.17360	0.18311	0.1938

Table 4. Comparison of mode (*m*, *n*) = (1, 1) C-F SWCNTs frequencies.

	Frequencies (THz)		
L/d	Present	WPA [23]	MD Simulation [18]
4.67	0.13586	0.17074	0.23193
6.47	0.07197	0.09048	0.12872
7.55	0.05311	0.06678	0.10000
8.28	0.04426	0.05566	0.07935
10.07	0.03004	0.03777	0.05493
13.69	0.01631	0.02051	0.03052
17.30	0.01023	0.01288	0.01831
20.89	0.00702	0.00883	0.01381
24.50	0.00510	0.00642	0.00916
28.07	0.00389	0.00489	0.00690
31.64	0.00306	0.00385	0.00610
35.34	0.00245	0.00309	0.00458

Table 5. Rotating SWCNT nondimensional frequencies $\chi_b, \chi_f = \omega R\sqrt{(1-\nu^2)\rho / E}$ with Ref.[68].

Ω		Method	n				
			2	3	4	5	6
0.01	χ_b	Chen et al.[68]	0.00163	0.00444	0.00842	0.01459	0.01993
		Present	0.00155	0.00438	0.00840	0.01335	0.01992
	χ_f	Chen et al.[68]	0.00162	0.00443	0.00841	0.01358	0.01993
		Present	0.00154	0.00437	0.00839	0.01358	0.01992

(χ_b, χ_f, designates the frequency of backward and forward frequency)

Table 6. Variations of natural frequencies (Hz) with *L/R*.

Type	*(m, n)*	Method	*L/R*				
			1	2	3	4	5
Zigzag	(8, 0)	backward	113.17	111.35	90.42	85.32	80.51
		forward	113.01	111.13	90.22	85.22	80.21
Chiral	(9, 5)	backward	1201.12	812.71	544.18	513.76	504.45
		forward	1201.03	812.66	544.05	513.23	504.19

Table 7. Variations of natural frequencies (Hz) with *h/R*.

Type	*(m, n)*	Method	*h/R*				
			0.001	0.002	0.003	0.004	0.005
Zigzag	(8, 0)	backward	21.44	22.04	22.69	22.98	23.52
		forward	21.33	21.92	22.48	22.76	23.41
Chiral	(9, 5)	backward	101.01	104.118	108.452	114.682	116.28
		forward	100.87	104.109	108.432	114.639	116.18

Table 8. Variations of natural frequencies (Hz) with Ω.

Type	*(m, n)*	Method	Ω				
			0	1	2	3	4
Zigzag	(8, 0)	backward	20.10	20.14	21.19	22.23	23.28
		forward	20.10	19.25	18.48	17.61	16.79
Chiral	(9, 5)	backward	33.45	33.61	34.23	34.44	35.48
		forward	33.45	33.04	32.79	32.38	32.09

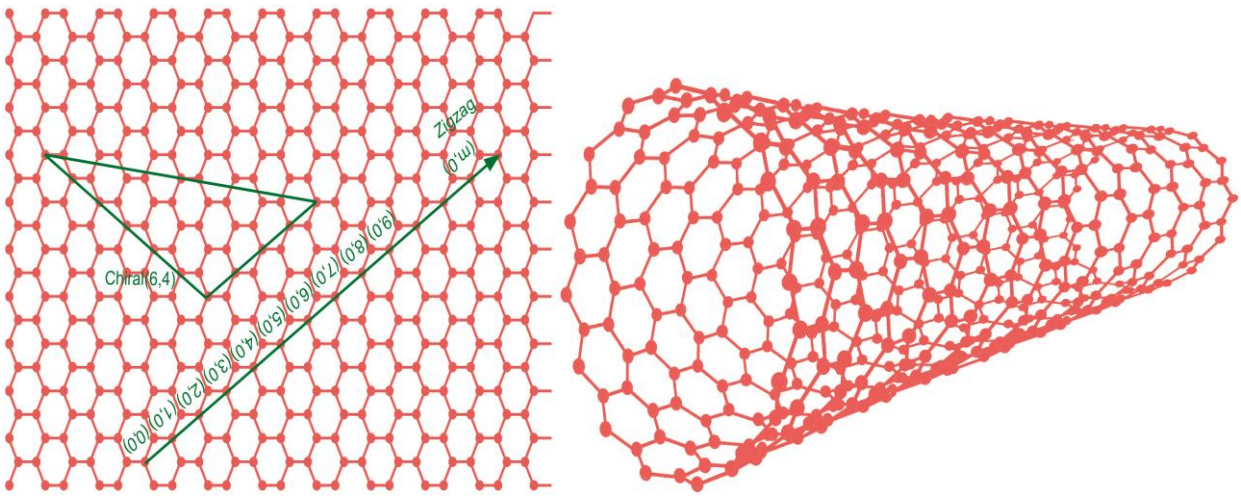

(a) (b)

Figure 1. (a) Schematic labeling of Graphene sheet (b) Rolling SWCNTs

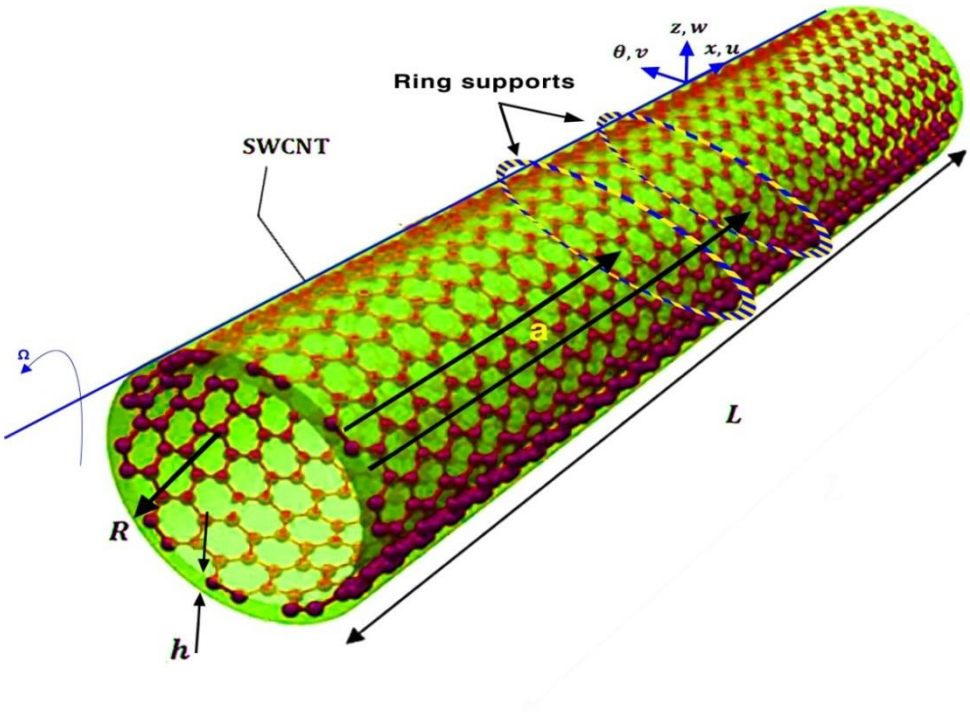

Figure 2. Rotating FG-CNT with geometrical sketch.

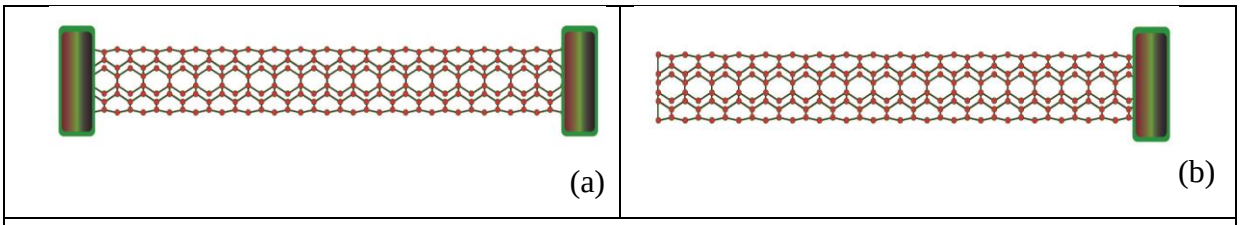

Figure 3. Schema of boundary conditions (a) C-C (b) C-F.

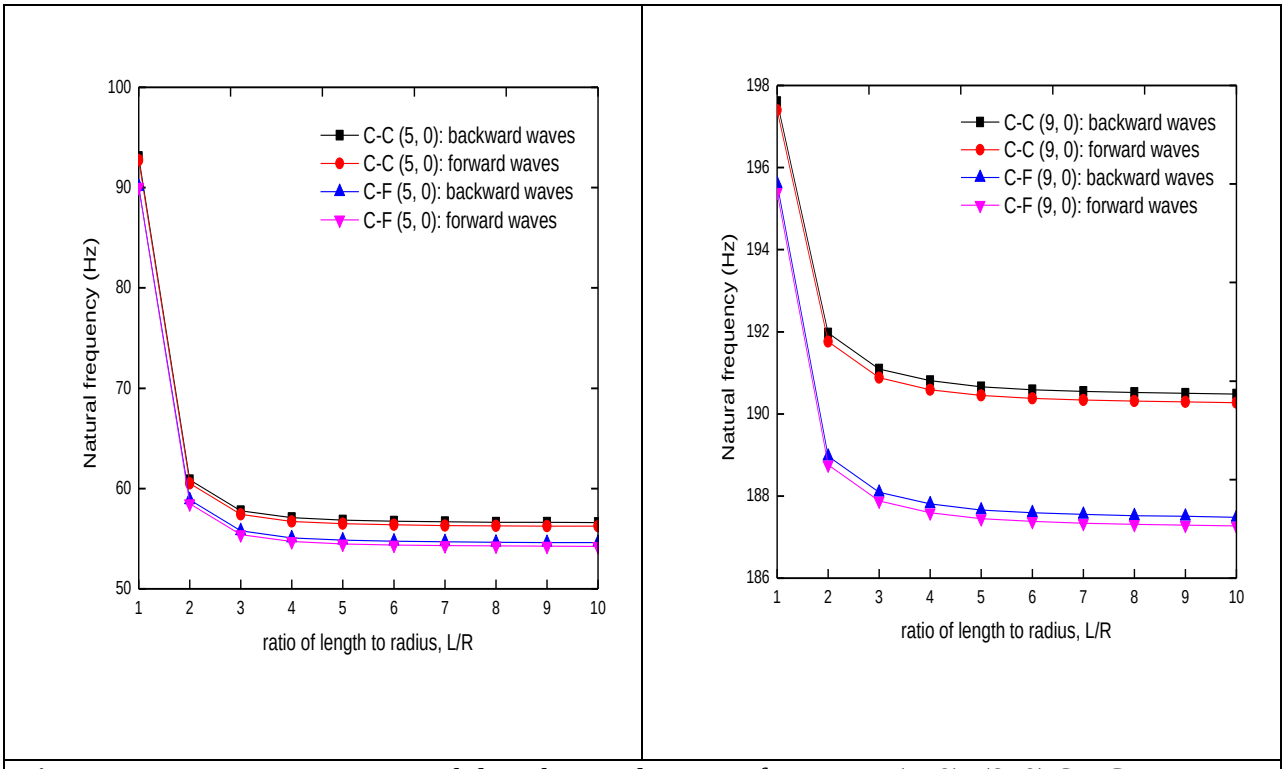

Figure 4. Frequency variation with length-to-radius ratio for zigzag (5, 0), (9, 0) SWCNTs.

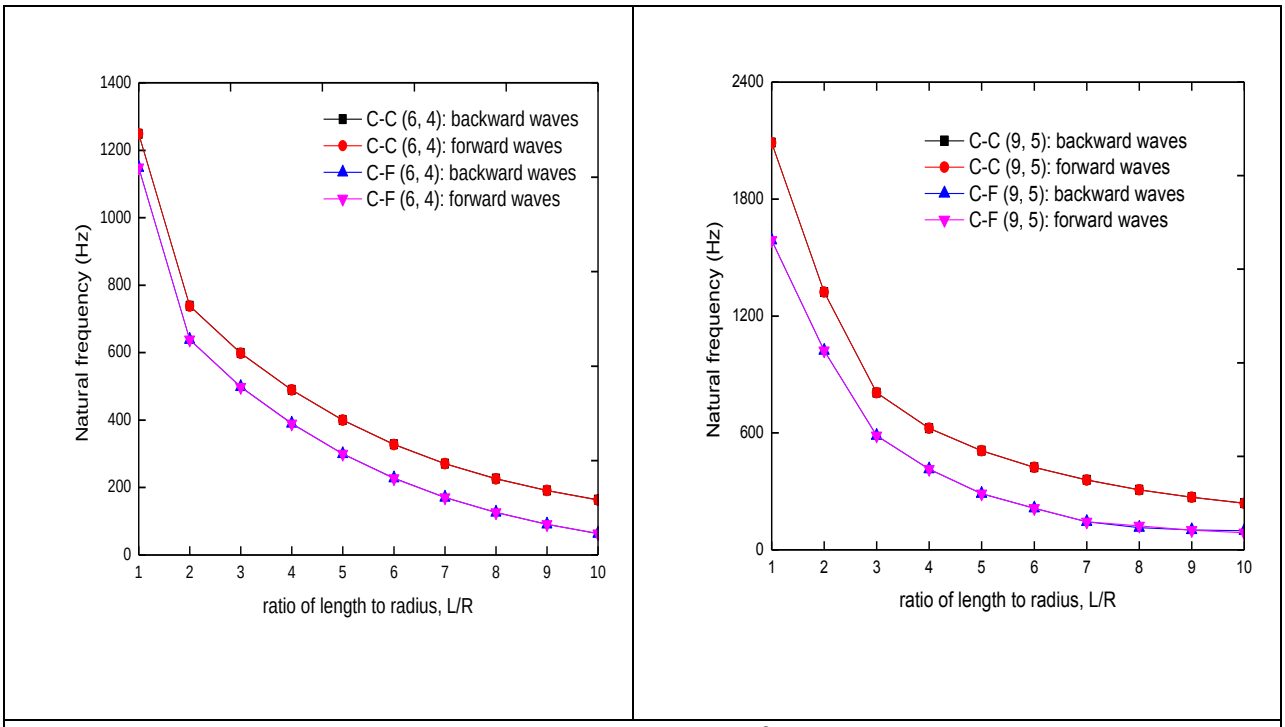

Figure 5. Frequency variation with length-to-radius ratio for chiral (6, 4), (9, 5) SWCNTs.

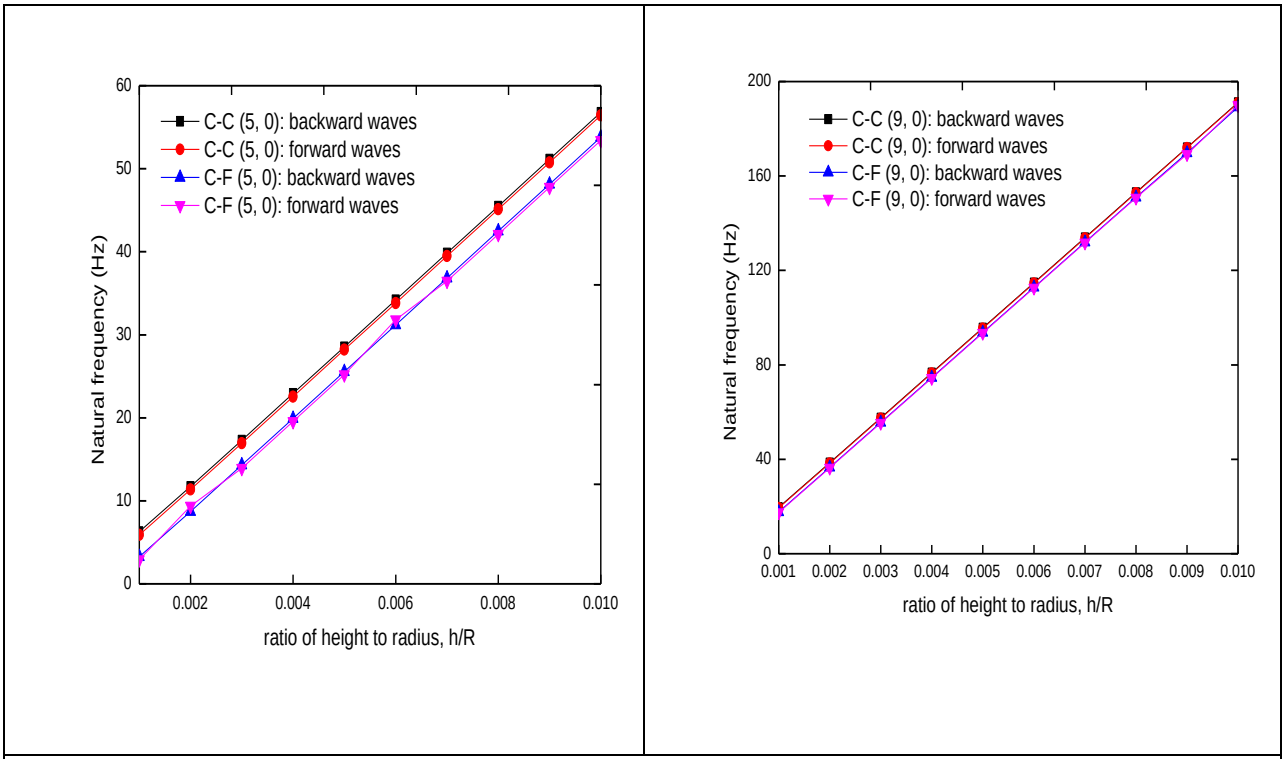

Figure 6. Frequency variation with height-to-radius ratio for zigzag (5, 0), (9, 0) SWCNTs.

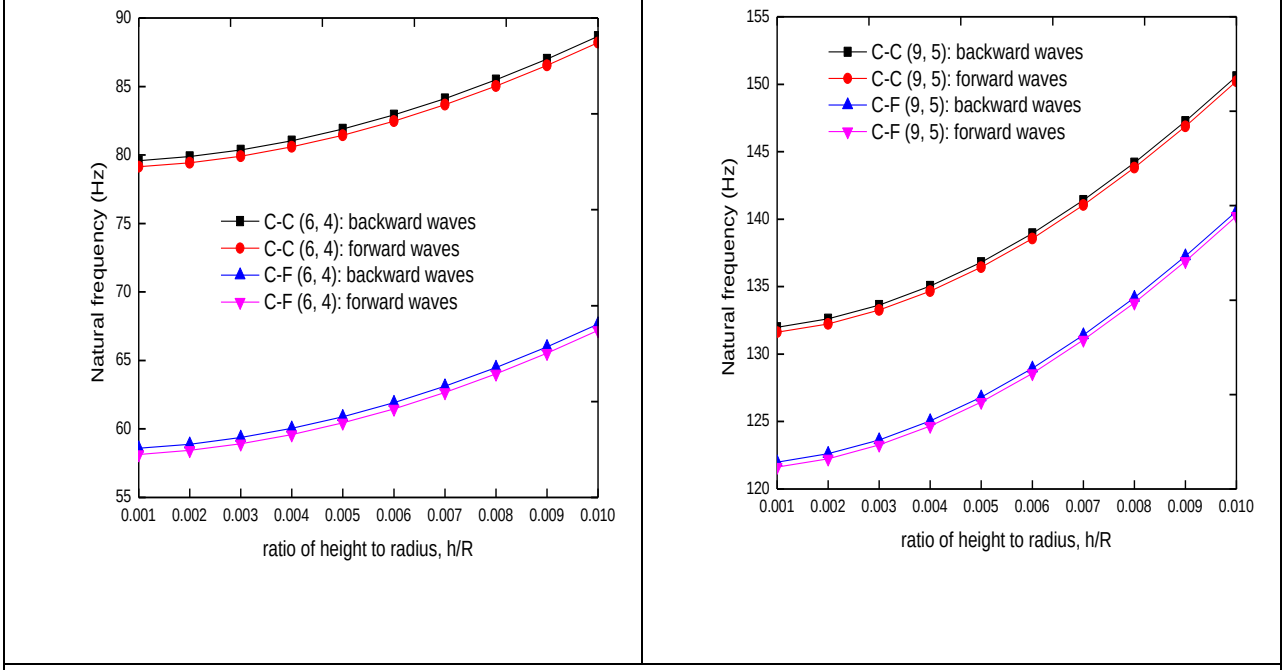

Figure 7. Frequency variation with height-to-radius ratio for chiral (6, 4), (9, 5) SWCNTs.

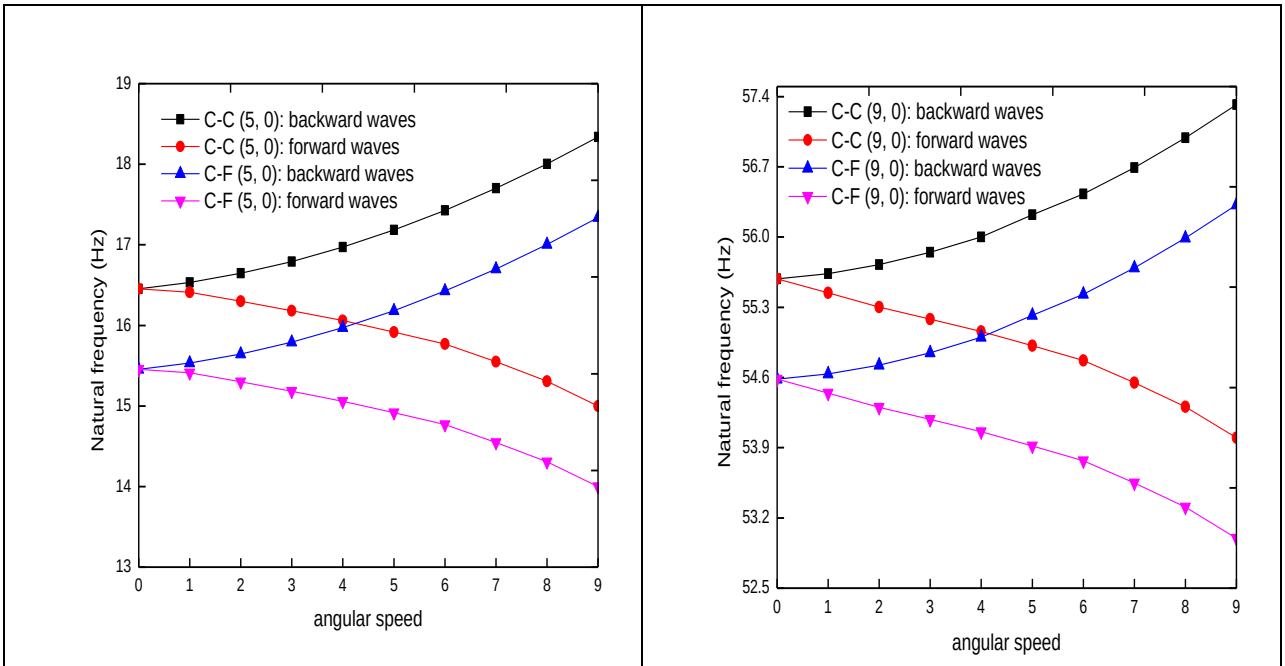

Figure 8. Frequency variation with angular speed for zigzag (5, 0), (9, 0) SWCNTs.

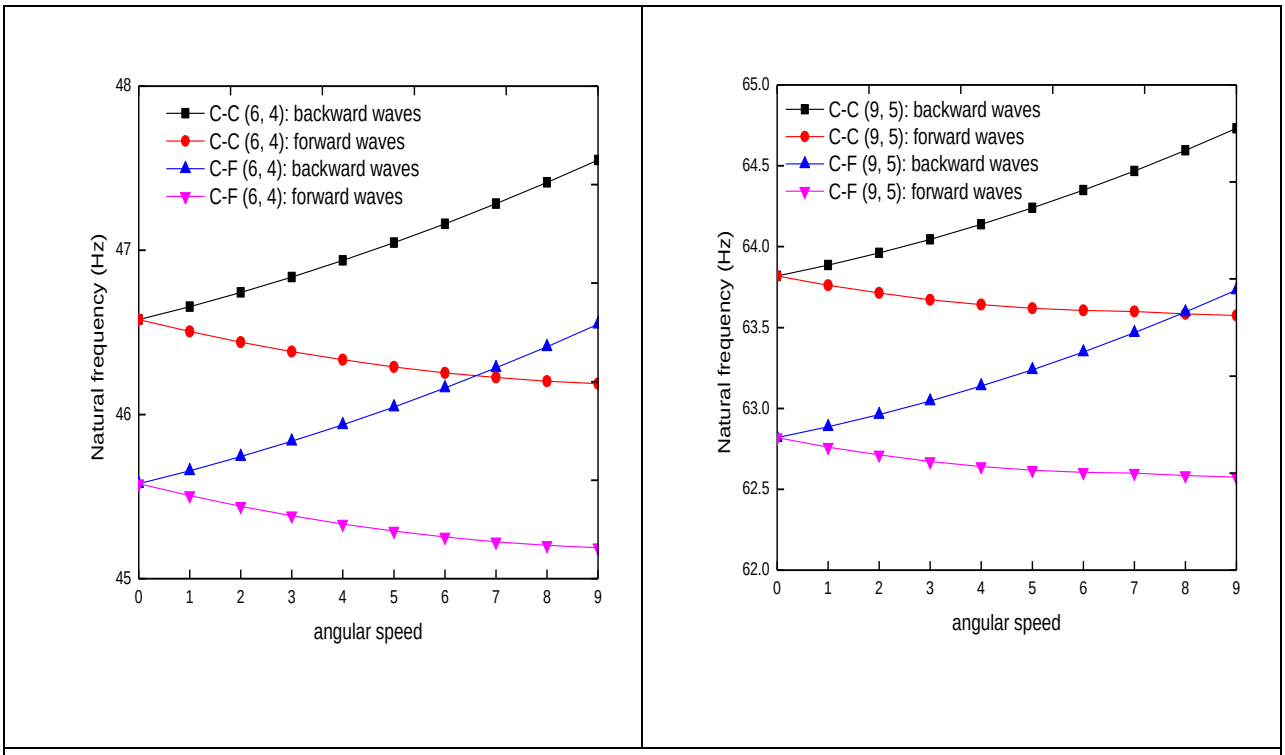

Figure 9. Frequency variation with angular speed for chiral (6, 4), (9, 5) SWCNTs.

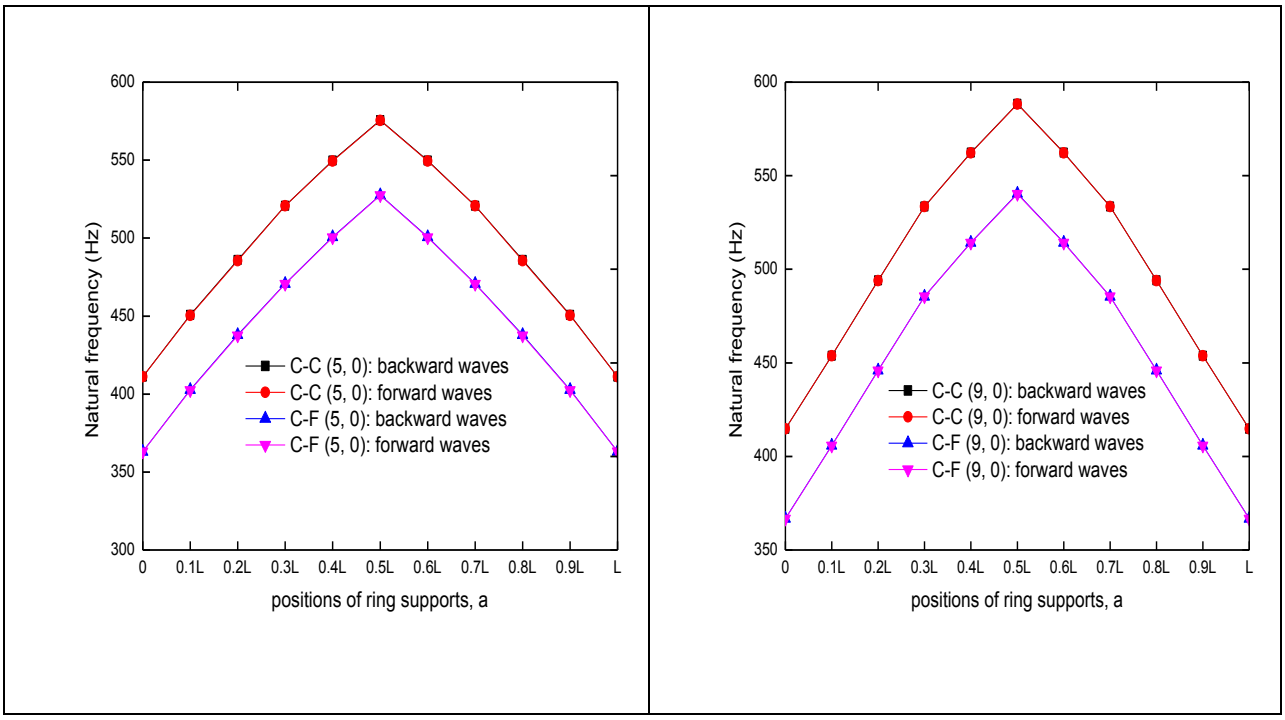

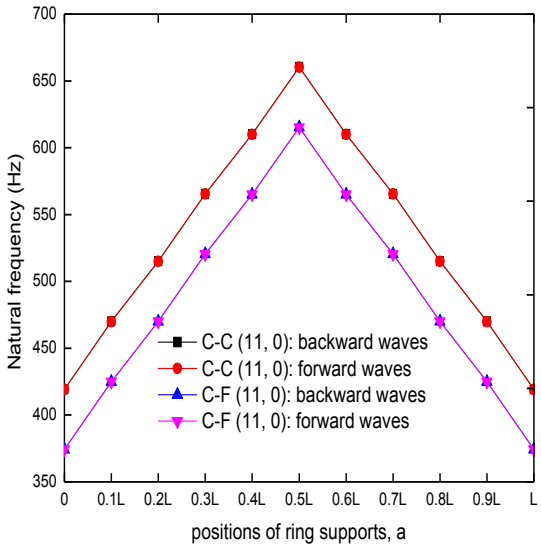

Figure 10. Frequency variation with ring supports of zigzag (5, 0), (9, 0), (11, 0).

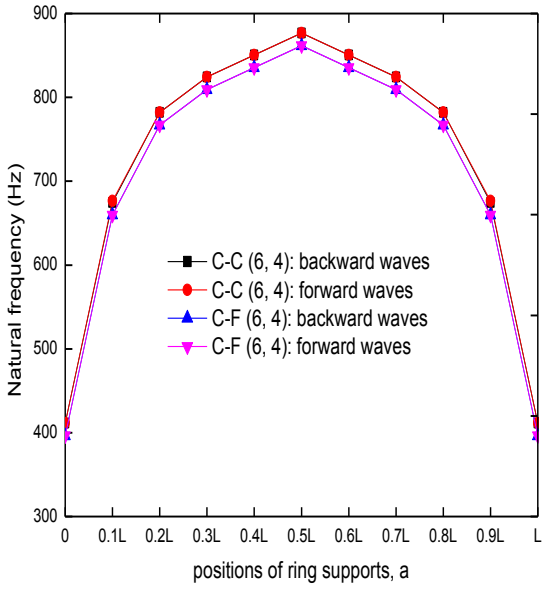

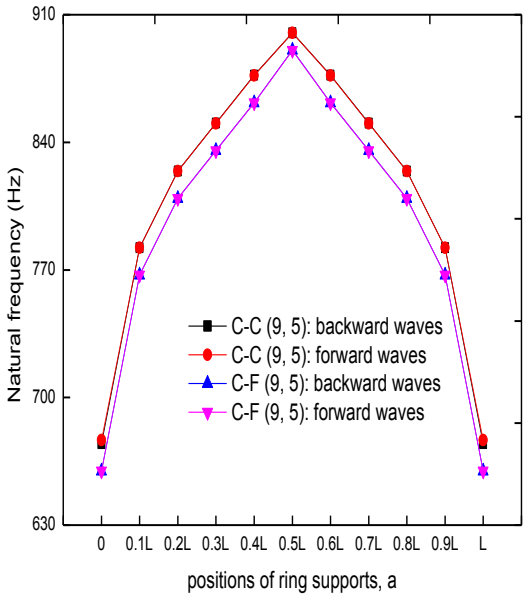

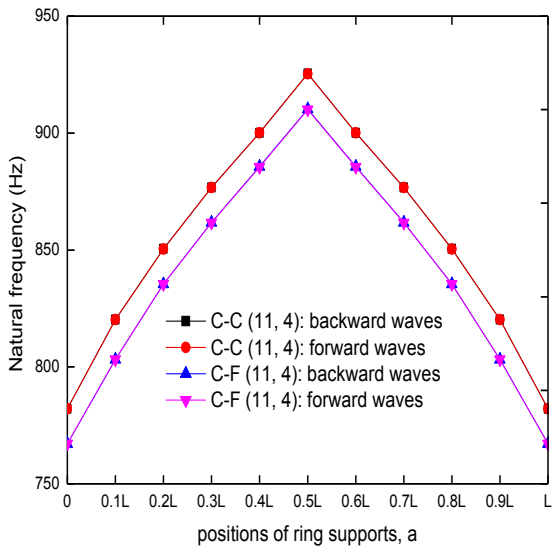

Figure 11. Frequency variation with ring supports of chiral SWCNTs (6, 4), (9, 5), (11, 4).